Received: 4 January 2023 | Revised: 25 July 2023 | Accepted: 19 August 2023

DOI: 10.1002/cnm.3771

APPLIED RESEARCH

WILEY

An aneurysm-specific preconditioning technique for the acceleration of Newton-Krylov method with application in the simulation of blood flows

Yingzhi Liu | **Fenfen Qi** | **Xiao-Chuan Cai**

Department of Mathematics, University of Macau, Macau, People's Republic of China

Correspondence
Xiao-Chuan Cai, Department of Mathematics, University of Macau, Macau, People's Republic of China.
Email: xccai@um.edu.mo

Funding information
NSFC, Grant/Award Number: 12201658; FDCT, Grant/Award Numbers: 0079/2021/AFJ, 0141/2021/A3

Abstract

In this paper, we develop an algorithm to simulate blood flows in aneurysmal arteries and focus on the construction of robust and efficient multilevel preconditioners to speed up the convergence of both linear and nonlinear solvers. The work is motivated by the observation that in the local aneurysmal region, the flow is often quite complicated with one or more vortices, but in the healthy section of the artery, the principal component of blood flows along the centerline of the artery. Based on this observation, we introduce a novel two-level additive Schwarz method with a mixed-dimensional coarse preconditioner. The key components of the preconditioner include (1) a three-dimensional coarse preconditioner covering the aneurysm; (2) a one-dimensional coarse preconditioner covering the central line of the healthy section of the artery; (3) a collection of three-dimensional overlapping subdomain preconditioners covering the fine meshes of the entire artery; (4) extension/restriction operators constructed by radial basis functions. The blood flow is modeled by the unsteady incompressible Navier–Stokes equations with resistance outflow boundary conditions discretized by a stabilized finite element method on fully unstructured meshes and the second-order backward differentiation formula in time. The resulting large nonlinear algebraic systems are solved by a Newton-Krylov algorithm accelerated by the new preconditioner in two ways: (1) the initial guess of Newton is obtained by solving a linear system defined by the coarse preconditioner; (2) the Krylov solver of the Jacobian system is preconditioned by the new preconditioner. Numerical experiments indicate that the proposed preconditioner is highly effective and robust for complex flows in a patient-specific artery with aneurysm, and it significantly reduces the numbers of linear and nonlinear iterations.

KEYWORDS

blood flows in aneurysmal artery, fully implicit finite element, mixed-dimensional coarse preconditioner, two-level Schwarz, unsteady incompressible Navier–Stokes problem

1 | INTRODUCTION

Computational hemodynamics is an important tool to study the behavior of blood flows and help understand certain vascular diseases such as the effect of the flow patterns and the distribution of the wall shear stress on the growth of the cerebral aneurysm.[1,2] With the rapid development of supercomputing and parallel algorithms in recent years, computational fluid dynamics (CFD) based technology for blood flow studies is becoming a powerful tool for research and clinic studies.[3–10] Compared with the standard imaging technologies such as computed tomography, magnetic resonance imaging, and transcranial Doppler, the CFD-based methods provide more details of blood flows. In the CFD modeling, 3D unsteady incompressible Navier–Stokes equations with suitable initial and boundary conditions[11–13] are commonly used, and the arterial geometry is extracted from medical images. Because of the complexity of the incompressible Navier–Stokes equations and the complex patient-specific geometry, the CFD-based methods often take a great deal of compute time. To reduce the total compute time is essential in order to apply the methods in clinical situations. In the methods, the system of partial differential equations is first discretized in space and time and then solved using a Newton-Krylov method[14] in which an inexact Newton method[15] is used to solve the nonlinear system, and a Krylov subspace method[16] is used to solve the linear Jacobian system at each Newton step. The robustness and effectiveness of the Krylov subspace method depend on a suitable preconditioner, and the fast convergence of the inexact Newton method requires a sufficiently good initial guess. In this paper, we introduce a mixed-dimensional coarse approximation of the incompressible Navier–Stokes operator that can be used to provide a good initial guess for Newton and a good second-level preconditioner for the Krylov iteration.

There are several classes of preconditioning methods for the incompressible Navier–Stokes equations such as block preconditioners and domain decomposition preconditioners. Among block preconditioners, Klawonn introduced block-diagonal and block-triangular preconditioners based on the block structure of the discretized matrix,[17,18] and Quarteroni et al.,[19,20] Elman et al.,[21–23] and Benzi et al.[24,25] developed block preconditioners based on the algebraic factorization methods. Among domain decomposition preconditioners, Klawonn et al.[26] and Li et al.[27] presented nonoverlapping substructuring preconditioners, and Klawonn et al.[28,29] and Cai et al.[3,30] introduced monolithic overlapping additive Schwarz preconditioners. We should mention that there are other methods such as multigrid methods,[31] lattice Boltzmann methods,[32] and isogeometric methods.[33] In this paper, we focus on the additive Schwarz preconditioner which is a powerful and naturally parallel preconditioner, but the scalability of the one-level preconditioner is not guaranteed when the number of subdomains increases.[34,35] To improve the scalability we introduce a special coarse space for the two-level additive Schwarz preconditioner for the 3D unsteady incompressible Navier–Stokes equations in a patient-specific cerebral artery with aneurysm.

Recently, we designed a robust and efficient two-level additive Schwarz preconditioner with a 1D coarse preconditioner for 2D steady-state Stokes equations in artery-like domains[36] and 3D unsteady incompressible Stokes and Navier–Stokes equations in patient-specific arteries.[37,38] The key components of the 1D coarse preconditioner include a coarse global matrix obtained by a finite element discretization of parameterized 1D Stokes and Navier–Stokes models, a 3D-to-1D restriction matrix and a 1D-to-3D extension matrix constructed by some approximation techniques. The most attractive feature of the method is that its computational cost is nearly negligible. The 1D model is obtained by the homogenization of the 3D Navier–Stokes equations on the axial cross-sections of the artery and the reduced order model has been applied to compute the averaged behavior of blood flows.[39–44] Instead of using the 1D model to simulate the entire flow, it can also be used as coarse preconditioners for some patient-specific arteries even with a large number of branches. However, for arteries with moderate to large size aneurysm, our numerical experiments show that the performance of the 1D coarse preconditioner degrades significantly because it is impossible to define a reasonable centerline in the aneurysmal region.

To overcome the difficulty, we propose a new method that combines the 1D coarse preconditioner defined on the centerline of the normal region with a 3D coarse preconditioner[3] defined on the small 3D aneurysmal region to form a mixed-dimensional coarse preconditioner with some compatibility conditions on the interfaces of the centerline and the aneurysm. The mixed-dimensional Navier–Stokes model is discretized in space by a stabilized finite element method on the coarse mesh and the implicit backward Euler method in time. This mixed-dimensional coarse problem serves two different purposes: (1) to reduce the number of linear iterations in the Krylov subspace method; (2) to reduce the number of nonlinear iterations in the inexact Newton method. Different from most initial-boundary value problems, the initial condition for the blood flow problem is not actually available since a direct measurement of the entire flow field at any given moment is clinically impossible, therefore, in traditional simulations, an approximate initial condition is used that involves the Dirichlet boundary values for the boundary points and zero values for all other mesh points. Such a "Dirichlet+zero" initial condition is also used to obtain the initial guess for the inexact Newton method for the first time step, which often results in a large number of iterations. In this work, a new initial guess for the

inexact Newton method is derived by solving the mixed-dimensional coarse preconditioning system with a special right-hand side defined using the nonlinear residual function computed with the "Dirichlet+zero" initial condition.

The rest of the paper is organized as follows. In Section 2 we describe the model problem and the stabilized finite element discretization. In Section 3 we derive the mixed-dimensional Navier–Stokes model with compatibility conditions on the 1D and 3D interface. In Section 4, we develop the two-level additive Schwarz preconditioner with the mixed-dimensional coarse preconditioner. In Section 5 we discuss a method that uses the mixed-dimensional coarse problem to initialize the inexact Newton iteration. Section 6 shows some numerical experiments for a patient-specific aneurysmal artery and some conclusions are given in Section 7.

2 | MODEL PROBLEM AND ITS DISCRETIZATION

In an aneurysmal artery $\Omega \in \mathbb{R}^3$ (see Figure 1), we consider the unsteady incompressible Navier–Stokes problem

$$\begin{cases} \rho\left(\dfrac{\partial \boldsymbol{u}}{\partial t} + \boldsymbol{u}\cdot\nabla\boldsymbol{u}\right) - \mu\Delta\boldsymbol{u} + \nabla p = \boldsymbol{0} & \text{in } \Omega\times(0,T), \\ \nabla\cdot\boldsymbol{u} = 0 & \text{in } \Omega\times(0,T), \\ \boldsymbol{u}(x,0) = \boldsymbol{0} & \text{in } \Omega, \\ \boldsymbol{u} = \boldsymbol{u}_I & \text{on } \Gamma_I\times(0,T), \\ \boldsymbol{u} = \boldsymbol{0} & \text{on } \Gamma_W\times(0,T), \\ p = R_O^i Q_O^i & \text{on } \Gamma_O^i\times(0,T), i=1,\ldots,m, \end{cases} \tag{1}$$

where $\boldsymbol{u} = (u_1,u_2,u_3)^T$ is the blood velocity and p is the blood pressure, μ is the dynamic viscosity, and ρ is the blood density. On the boundary, we impose a velocity Dirichlet condition on the inlet Γ_I, a non-slip condition on the wall Γ_W, and a resistance condition on the outlets $\Gamma_O = \bigcup_{i=1}^{m}\Gamma_O^i$, where m is the number of outlets. Here R_O^i is the constant resistance and $Q_O^i = \int_{\Gamma_O^i}\boldsymbol{u}\cdot\boldsymbol{n}\mathrm{d}\Gamma_O^i$ is the flux on Γ_O^i with the outward unit normal vector $\boldsymbol{n}$.

Define $\boldsymbol{V}(\Omega) = \left\{\boldsymbol{v}\in\boldsymbol{H}^1(\Omega):\boldsymbol{v}|_{\Gamma_I} = \boldsymbol{u}_I, \boldsymbol{v}|_{\Gamma_W} = 0\right\}$, $\boldsymbol{V}_0(\Omega) = \left\{\boldsymbol{v}\in\boldsymbol{H}^1(\Omega):\boldsymbol{v}|_{\Gamma_I\cup\Gamma_W} = 0\right\}$. Denote $(u,v) = \int_\Omega uv\mathrm{d}\Omega$, $\langle u,v\rangle_{\Gamma_O} = \int_{\Gamma_O} uv\mathrm{d}\Gamma_O$. Then the variational formulation of (1) is to find $(\boldsymbol{u}(\cdot,t),p(\cdot,t))\in\boldsymbol{V}(\Omega)\times L^2(\Omega)$ such that

$$\begin{aligned} &\left(\rho\frac{\partial\boldsymbol{u}}{\partial t},\boldsymbol{v}\right) + (\mu\nabla\boldsymbol{u},\nabla\boldsymbol{v}) - (p,\nabla\cdot\boldsymbol{v}) + (q,\nabla\cdot\boldsymbol{u}) + (\rho\boldsymbol{u}\cdot\nabla\boldsymbol{u},\boldsymbol{v}) \\ &-\langle\mu\nabla\boldsymbol{u}\cdot\boldsymbol{n},\boldsymbol{v}\rangle_{\Gamma_O} + \sum_{i=1}^{m} R_O^i\int_{\Gamma_O^i}\boldsymbol{u}\cdot\boldsymbol{n}\mathrm{d}\Gamma_O^i\int_{\Gamma_O^i}\boldsymbol{v}\cdot\boldsymbol{n}\mathrm{d}\Gamma_O^i = 0, \end{aligned} \tag{2}$$

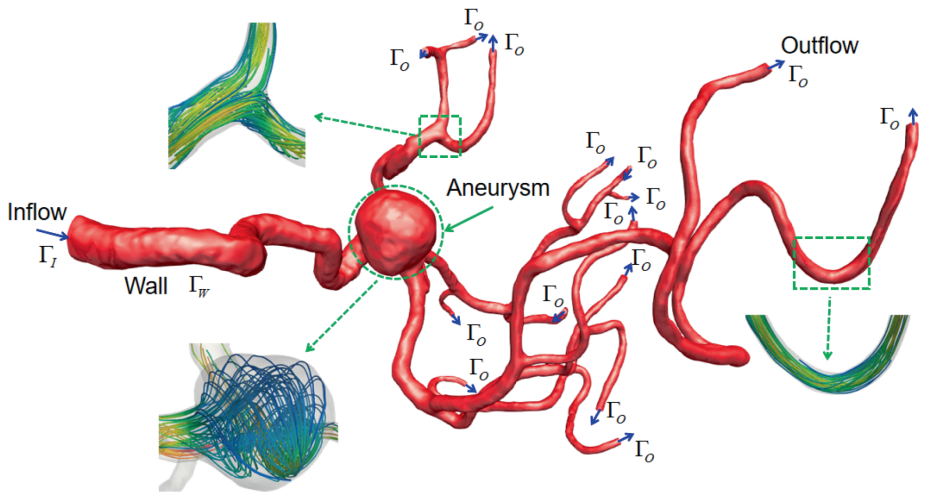

FIGURE 1 An aneurysmal artery with 1 inlet and 15 outlets and flow patterns at aneurysmal, bifurcating and normal regions.

for all $(\boldsymbol{v},q)\in \boldsymbol{V}_0(\Omega)\times L^2(\Omega)$ and $t\in(0,T)$. Let $\mathcal{T}_h$ be a shape-regular unstructured tetrahedral mesh of Ω, and S_h the continuous, piecewise linear polynomial function space on $\mathcal{T}_h$. The P1-P1 finite element method is used and the finite element spaces are as follows

$$\boldsymbol{V}_h=[S_h]^3\cap\boldsymbol{V}(\Omega),\boldsymbol{W}_h=[S_h]^3\cap\boldsymbol{V}_0(\Omega),Q_h=S_h\cap L^2(\Omega).$$

As the finite element pair $(\boldsymbol{W}_h,Q_h)$ does not satisfy the inf-sup condition,[45] we use the stabilized finite element method[3,46] to spatially discretize the weak formulation (2): find $(\boldsymbol{u}_h(\cdot,t),p_h(\cdot,t))\in\boldsymbol{V}_h\times Q_h$, such that

$$\begin{cases}\left(\rho\dfrac{\partial\boldsymbol{u}_h}{\partial t},\boldsymbol{v}_h\right)+(\mu\nabla\boldsymbol{u}_h,\nabla\boldsymbol{v}_h)-(p_h,\nabla\cdot\boldsymbol{v}_h)+(q_h,\nabla\cdot\boldsymbol{u}_h)+(\rho\boldsymbol{u}_h\cdot\nabla\boldsymbol{u}_h,\boldsymbol{v}_h)\\ -\langle\mu\nabla\boldsymbol{u}_h\cdot\boldsymbol{n},\boldsymbol{v}_h\rangle_{\Gamma_O}+\sum\limits_{i=1}^{m}R_O^i\int_{\Gamma_O^i}\boldsymbol{u}_h\cdot\boldsymbol{n}\mathrm{d}\Gamma_O^i\int_{\Gamma_O^i}\mathbf{v}_h\cdot\boldsymbol{n}\mathrm{d}\Gamma_O^i+\sum\limits_{K\in\mathcal{T}_h}(\nabla\cdot\boldsymbol{u}_h,\gamma_2\nabla\cdot\boldsymbol{v}_h)_K\\ +\sum\limits_{K\in\mathcal{T}_h}\left(\rho\left(\frac{\partial\boldsymbol{u}_h}{\partial t}+\boldsymbol{u}_h\cdot\nabla\boldsymbol{u}_h\right)+\nabla p_h,\gamma_1(\boldsymbol{u}_h\cdot\nabla\boldsymbol{v}_h+\nabla q_h)\right)_K=0,\end{cases}\tag{3}$$

for all $(\boldsymbol{v}_h,q_h)\in\boldsymbol{W}_h\times Q_h$ and $t\in(0,T)$, where γ_1 and γ_2 are the stabilization parameters satisfying

$$\gamma_1=\left(\sqrt{\frac{4}{\Delta t^2}+\boldsymbol{u}_h^T\boldsymbol{G}\boldsymbol{u}_h+36\left(\frac{\mu}{\rho}\right)^2\boldsymbol{G}:\boldsymbol{G}}\right)^{-1},\gamma_2=\left(8\gamma_1\sum_{i=1}^{3}\mathrm{G}_{i,i}\right)^{-1},$$

here $\boldsymbol{G}=(\mathrm{G}_{i,j}),(i,j=1,2,3)$ satisfies $\mathrm{G}_{i,j}=\sum_{k=1}^{3}\frac{\partial\widehat{x_k}}{\partial x_i}\frac{\partial\widehat{x_k}}{\partial x_j}$, where $\{\widehat{x}_i\}_{i=1}^3$ and $\{x_i\}_{i=1}^3$ are the local reference and global physical coordinate variables, respectively. Let $(\boldsymbol{u}_h,p_h)$ be the solution of (3). Denote the unknowns vectors of $\boldsymbol{u}_h$ and p_h as (U,V,W) and P, respectively. Then the semi-discretized system (3) can be rewritten as a system of ordinary differential equations

$$\frac{dX}{dt}=L(X),\tag{4}$$

where $X=(U,V,W,P)^T$ is the time-dependent unknown vector. We subdivide the time interval $(0,T)$ with a fixed time step size Δt and use the second-order backward differentiation formula (BDF2) for the temporal discretization to (4). Then we obtain a fully discretized system at $t_n=n\Delta t$

$$\frac{\frac{3}{2}X^n-2X^{n-1}+\frac{1}{2}X^{n-2}}{\Delta t}=L(X^n),\quad(n\geq2)\tag{5}$$

where X^1 is obtained by the first-order implicit backward Euler method.

Rewrite the nonlinear system (5) as

$$F^n(X^n)=0.\tag{6}$$

The nonlinear algebraic system (5) is often large and sparse for a high-resolution simulation of blood flows, and we solve it by a Newton-Krylov method. Specifically, in the outer iteration, an inexact Newton method is used to update the numerical solution of (6) and in the inner iteration, the linear Jacobian system is approximately solved by a Krylov subspace method to approximate the Newton direction. Note that the Jacobian system is a Stokes-like system and has the same dimension as the nonlinear system (6). The most time-consuming part of the computation is solving the Jacobian systems, therefore, it is necessary to design an efficient preconditioner. There are many general purpose preconditioners,[3,30] but they require a coarse mesh that has to be sufficiently fine to resolve the geometry of the fine mesh. Consequently the computational time spent on the coarse mesh is very high and their performance is not

satisfactory. We therefore introduce a method designed particularly for the time-dependent Navier–Stokes problem defined on an arterial domain with aneurysm. In the following sections, we first introduce a two-level additive Schwarz preconditioner with a mixed-dimensional coarse preconditioner for the Jacobian system. Then, we propose a mixed-dimensional coarse correction to generate a better initial guess for the inexact Newton method.

3 | A MIXED-DIMENSIONAL NAVIER–STOKES MODEL AND ITS DISCRETIZATION

In this section, we introduce a mixed-dimensional Navier–Stokes model obtained by coupling a 1D Navier–Stokes model defined on the centerline of the normal region with a 3D Navier–Stokes model defined in the aneurysmal region with some suitable interface conditions. The new model will be used to construct a better initial guess for Newton and also a better coarse preconditioner for the Jacobian solver.

We divide Ω into a normal region Ω_o and an aneurysmal region Ω_a and denote $\Gamma = \partial\Omega_o \cap \partial\Omega_a$ as the interface, see the left subfigure of Figure 2. Let Ω_o^{cl} be the centerline of Ω_o, s_I the center of Γ_I and $\{s_O^i\}_{i=1}^m$ the center of $\{\Gamma_O^i\}_{i=1}^m$.

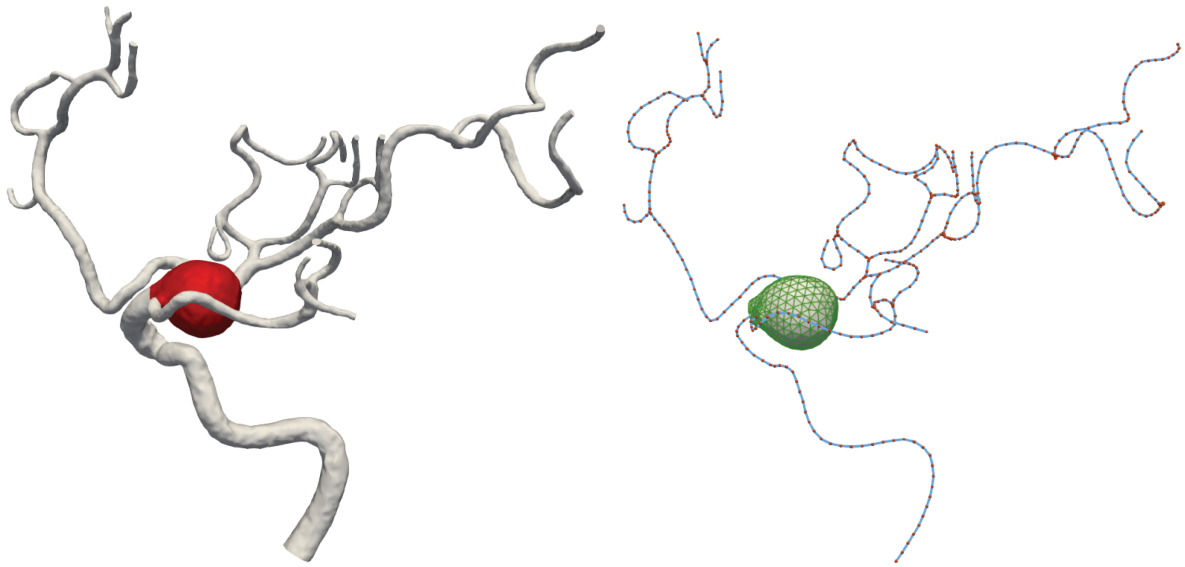

FIGURE 2 Normal (gray) and aneurysmal (red) regions of an aneurysmal artery (left) and the corresponding mixed-dimensional domain with a mixed-dimensional coarse mesh.

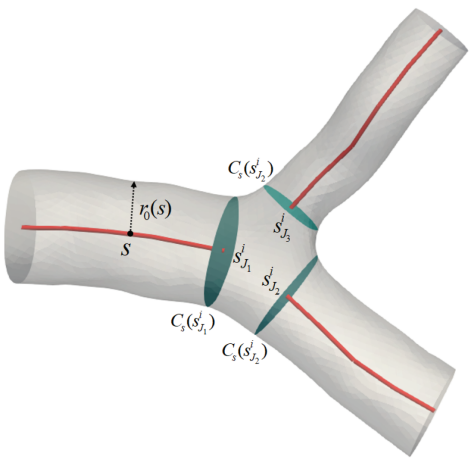

FIGURE 3 Centerline of an artery at a bifurcation and some notations.

Denote by m_{cl} the number of branches of Ω_o^{cl} and m_J the number of bifurcations of Ω_o^{cl}. On each bifurcation, without loss of generality, we assume that there is one inflow branch and two outflow branches and denote the corresponding adjoining points by $\left\{s_{J_1}^i\right\}_{i=1}^{m_J}$ and $\left\{\left(s_{J_2}^i, s_{J_3}^i\right)\right\}_{i=1}^{m_J}$, see Figure 3. Then the mixed-dimensional model defined in $\Omega_o^{cl} \cup \Omega_a$ (see the right subfigure of Figure 2) can be described as follows.[39,47,48]

1. On the centerline Ω_o^{cl}, we consider the 1D Navier–Stokes equations[38,40,41]

$$\begin{cases} \rho\dfrac{A_s}{2}\dfrac{\partial u^{cl}}{\partial t}+\beta\rho\dfrac{\alpha}{4}A_s u^{cl}\dfrac{\partial u^{cl}}{\partial s}+\dfrac{K_r}{2}u^{cl}+A_s\dfrac{\partial p^{cl}}{\partial s}=0 \text{ in}\Omega_o^{cl}\times(0,T), \\ \dfrac{\partial}{\partial s}\left(A_s u^{cl}\right)=0 \text{ in } \Omega_o^{cl}\times(0,T), \\ u^{cl}(s,0)=0 \text{ in } \Omega_o^{cl}, \end{cases} \tag{7}$$

with the boundary conditions

$$u^{cl}(s_I,t)=-\frac{2}{|\Gamma_I|}\int_{\Gamma_I}\boldsymbol{u}_I\cdot\boldsymbol{n}\mathrm{d}\Gamma_I,\quad p^{cl}\left(s_O^i,t\right)=\frac{R_O^i A_s}{2}u^{cl}\left(s_O^i,t\right)\quad (i=1,...,m), \tag{8}$$

and the bifurcation compatibility conditions

$$A_s\left(s_{J_1}^i\right)u^{cl}\left(s_{J_1}^i\right)=A_s\left(s_{J_2}^i\right)u^{cl}\left(s_{J_2}^i\right)+A_s\left(s_{J_3}^i\right)u^{cl}\left(s_{J_3}^i\right), \tag{9}$$

$$p^{cl}\left(s_{J_1}^i\right)=p^{cl}\left(s_{J_2}^i\right)=p^{cl}\left(s_{J_3}^i\right)(i=1,...,m_J), \tag{10}$$

where $\alpha=4/3$ is the Coriolis coefficient and $K_r=8\pi\mu$. Here β is a model parameter and corresponds to the Stokes model ($\beta=0$) and the Navier–Stokes model ($\beta=1$).

2. In the aneurysmal region Ω_a, we consider the 3D Navier–Stokes equations

$$\begin{cases} \rho\left(\dfrac{\partial\boldsymbol{u}}{\partial t}+\beta\boldsymbol{u}\cdot\nabla\boldsymbol{u}\right)-\mu\Delta\boldsymbol{u}+\nabla p=0 \text{ in } \Omega_a\times(0,T), \\ \nabla\cdot\boldsymbol{u}=0 \text{ in } \Omega_a\times(0,T), \\ \boldsymbol{u}(x,0)=0 \text{ in } \Omega_a, \\ \boldsymbol{u}=0 \text{ on } \partial\Omega_a\cap\Gamma_W\times(0,T). \end{cases} \tag{11}$$

3. On the interface $\Gamma=\bigcup_{i=1}^{m_f}\Gamma_i$, we consider the following compatibility conditions

$$u_i^{cl}=\mathrm{sign}(\boldsymbol{u}\cdot\boldsymbol{n})\frac{2}{|\Gamma_i|}\int_{\Gamma_i}\boldsymbol{u}\cdot\boldsymbol{n}\mathrm{d}\Gamma_i,\quad p_i^{cl}=\frac{1}{|\Gamma_i|}\int_{\Gamma_i}p\mathrm{d}\Gamma_i\ \left(i=1,...,m_f\right). \tag{12}$$

The first condition represents the conservation of mass across the interfaces, and the second condition shows the balance of forces from different sides of the interface.

Define $V\left(\Omega_o^{cl}\right)=\left\{v\in H^1\left(\Omega_o^{cl}\right):v(s_I)=-\frac{2}{|\Gamma_I|}\int_{\Gamma_I}\boldsymbol{u}_I\cdot\boldsymbol{n}\mathrm{d}\Gamma_I\right\}$ and $V_0\left(\Omega_o^{cl}\right)=\left\{v\in H^1\left(\Omega_o^{cl}\right):v\big|_{\partial\Omega_o^{cl}\setminus\Gamma}=0\right\}$ on the centerline of the normal region and $\boldsymbol{V}(\Omega_a)=\left\{\boldsymbol{v}\in\left[H^1(\Omega_a)\right]^3:\boldsymbol{v}\Big|_{\partial\Omega_a\cap\Gamma_W}=0\right\}$ in the aneurysmal region. The weak formulation of mixed-dimensional model (7)–(12) can be described as: find $\left(u^{cl}(\cdot,t),p^{cl}(\cdot,t)\right)\in V\left(\Omega_o^{cl}\right)\times L^2\left(\Omega_o^{cl}\right)$ and $(\boldsymbol{u}(\cdot,t),p(\cdot,t))\in\boldsymbol{V}(\Omega_a)\times L^2(\Omega_a)$, such that

$$\begin{cases} \left(\rho\frac{A_s}{2}\frac{\partial u^{cl}}{\partial t}+\frac{K_r}{2}u^{cl},v^{cl}\right)_{\Omega_o^{cl}}+\sum_{i=1}^{m_{cl}}A_s v^{cl}p^{cl}\Big|_{s_i^0}^{s_i^1}-\left(\frac{\partial A_s v^{cl}}{\partial s},p^{cl}\right)_{\Omega_o^{cl}} \\ +\beta\left(\rho\frac{\alpha}{4}A_s u^{cl}\frac{\partial u^{cl}}{\partial s},v^{cl}\right)_{\Omega_o^{cl}}+\eta\left(\frac{\partial A_s u^{cl}}{\partial s},q^{cl}\right)_{\Omega_o^{cl}}=0, \\ \rho\left(\frac{\partial \boldsymbol{u}}{\partial t}+\beta\boldsymbol{u}\cdot\nabla\boldsymbol{u},\boldsymbol{v}\right)_{\Omega_a}+\mu(\nabla\boldsymbol{u},\nabla\boldsymbol{v})_{\Omega_a}-(p,\nabla\cdot\boldsymbol{v})_{\Omega_a} \\ +(q,\nabla\cdot\boldsymbol{u})_{\Omega_a}+\sum_{i=1}^{m_f}p_i^{cl}\int_{\Gamma_i}\boldsymbol{v}\cdot\boldsymbol{n}\mathrm{d}\Gamma_i=0, \end{cases} \tag{13}$$

for all $(v^{cl},q^{cl})\in V_0(\Omega_o^{cl})\times L^2(\Omega_o^{cl})$, $(\mathbf{v},q)\in\mathbf{V}(\Omega_a)\times L^2(\Omega_a)$ and $t\in(0,T)$, where η is a positive parameter. In (13), the flux interface condition in (12) is used for the one-dimensional model (7) and the pressure interface condition in (12) is used for the three-dimensional model (11) which is a defective condition introduced in Reference 47.

Let $\mathcal{T}_H^{cl}$ be a polyline mesh of Ω_o^{cl} with the mesh size $O(H_{cl})$ and $\mathcal{T}_H^a$ a shape-regular unstructured tetrahedral mesh of Ω_a with the mesh size $O(H_a)$. Similarly, we denote S_H^{cl} and S_H^a as the continuous, piecewise linear polynomial function space on $\mathcal{T}_H^{cl}$ and $\mathcal{T}_H^a$, respectively, and the corresponding linear finite element spaces are defined as

$$V_H^{cl}=S_H^{cl}\cap V(\Omega_o^{cl}),W_H^{cl}=S_H^{cl}\cap V_0(\Omega_o^{cl}),Q_H^{cl}=S_H^{cl}\cap L^2(\Omega_o^{cl}),$$
$$\boldsymbol{V}_H^a=\left[S_H^a\right]^3\cap\boldsymbol{V}(\Omega_a),Q_H^a=S_H^a\cap L^2(\Omega_a).$$

Then, the stabilized finite element method to discretize (13) is to find $(u_H^{cl}(\cdot,t),p_H^{cl}(\cdot,t))\in V_H^{cl}\times Q_H^{cl}$ and $(\boldsymbol{u}_H(\cdot,t),p_H(\cdot,t))\in\boldsymbol{V}_H^a\times Q_H^a$, such that

$$\begin{cases} \left(\rho\frac{A_s}{2}\frac{\partial u_H^{cl}}{\partial t}+\frac{K_r}{2}u_H^{cl}+A_s\frac{\partial p_H^{cl}}{\partial s}+\beta\rho\frac{\alpha}{4}A_s u_H^{cl}\frac{\partial u_H^{cl}}{\partial s},v_H^{cl}\right)_{\Omega_o^{cl}}-\eta\left(A_s u_H^{cl},\frac{\partial q_H^{cl}}{\partial s}\right)_{\Omega_o^{cl}} \\ +\eta\sum_{i=1}^{m_{cl}}A_s u_H^{cl}q_H^{cl}\Big|_{s_i^0}^{s_i^1}+\gamma\sum_{e\in\mathcal{T}_H^{cl}}H_{cl}^2(e)\left(\rho\frac{A_s}{2}\frac{\partial u_H^{cl}}{\partial t}+\frac{K_r}{2}u_H^{cl}+A_s\frac{\partial p_H^{cl}}{\partial s},\frac{\partial q_H^{cl}}{\partial s}\right)_{\Omega_o^{cl}} \\ +\gamma\sum_{e\in\mathcal{T}_H^{cl}}H_{cl}^2(e)\left(\beta\rho\frac{\alpha}{4}A_s u_H^{cl}\frac{\partial u_H^{cl}}{\partial s},\frac{\partial q_H^{cl}}{\partial s}\right)_{\Omega_o^{cl}}=0, \\ \rho\left(\frac{\partial \boldsymbol{u}_H}{\partial t}+\beta\boldsymbol{u}_H\cdot\nabla\boldsymbol{u}_H,\boldsymbol{v}_H\right)_{\Omega_a}+\mu(\nabla\boldsymbol{u}_H,\nabla\boldsymbol{v}_H)_{\Omega_a}-(p_H,\nabla\cdot\boldsymbol{v}_H)_{\Omega_a}+\sum_{i=1}^{m_f}p_i^{cl}\int_{\Gamma_i}\boldsymbol{v}_H\cdot\boldsymbol{n}\mathrm{d}\Gamma_i \\ +(q_H,\nabla\cdot\boldsymbol{u}_H)_{\Omega_a}+\gamma\sum_{K\in\mathcal{T}_H^a}H_a^2(K)\left(\rho\left(\frac{\partial \boldsymbol{u}_H}{\partial t}+\beta\boldsymbol{u}_H\cdot\nabla\boldsymbol{u}_H\right)+\nabla p_H,\boldsymbol{u}_H\cdot\nabla\boldsymbol{v}_H+\nabla q_H\right)_K=0, \end{cases} \tag{14}$$

for all $(v_H^{cl},q_H^{cl})\in W_H^{cl}\times Q_H^{cl}$, $(\mathbf{v}_H,q_H)\in\boldsymbol{V}_H^a\times Q_H^a$ and $t\in(0,T)$, where γ is a positive stabilization parameter. For the time integration of (14), we use the implicit backward Euler method and obtain the nonlinear system at $t_n=n\Delta t$

$$F_{mc}^n(X_{mc}^n)=0, \tag{15}$$

where $X_{mc}^n=\left(X_{cl}^n,X_a^n\right)^T$ is the unknown vector at t_n, X_{cl}, and X_a correspond to the solutions of the 1D Navier–Stokes equations on Ω_o^{cl} and the 3D Navier–Stokes equations in Ω_a, respectively. Finally, the Jacobian matrix $A_{mc}^{n,k}$ of F_{mc}^n at the kth Newton solution $\left(X_{cl}^{n,k},X_a^{n,k}\right)$ takes the form

$$A_{mc}^{n,k}=\begin{pmatrix}A_{cl}\left(X_{cl}^{n,k}\right) & 2B_{31}^T\\ B_{31} & A_a\left(X_a^{n,k}\right)\end{pmatrix}, \tag{16}$$

where A_{cl} and A_a are the linearized discretized matrices of the 1D Navier–Stokes Equations (7)–(10) and the 3D Navier–Stokes Equation (11), respectively, and B_{31} corresponds to the interface integration $\sum_{i=1}^{m_f}p_i^{cl}\int_{\Gamma_i}\boldsymbol{v}_H\cdot\boldsymbol{n}\mathrm{d}\Gamma_i$.

In the next section we will use the Jacobian matrix (16) to construct a coarse preconditioner.

4 | TWO-LEVEL ADDITIVE SCHWARZ PRECONDITIONER WITH MIXED-DIMENSIONAL COARSE PRECONDITIONER

In this section, we introduce an overlapping two-level additive Schwarz preconditioner for the Jacobian problems corresponding to (6). The one-level additive Schwarz preconditioner is the sum of all the subdomain preconditioners and the coarse preconditioner is a combination of a 1D coarse preconditioner defined on the centerline of the normal region and a 3D coarse preconditioner defined in the aneurysmal region. In the following, we first briefly review the one-level method and then focus on the mixed-dimensional coarse preconditioner.

4.1 | One-level additive Schwarz preconditioner

To obtain the one-level additive Schwarz preconditioner, we first divide the arterial domain Ω into np non-overlapping subdomains $\{\Omega_i\}_{i=1}^{np}$ consisting of some elements of $\mathcal{T}_h$ denoted by $\{\mathcal{T}_{h,i}\}_{i=1}^{np}$. Then we extend the subdomains with δ layers of adjoining elements to overlapping subdomains $\{\Omega_i^\delta\}_{i=1}^{np}$ with the mesh $\mathcal{T}_{h,i}^\delta$ as follows

$$\mathcal{T}_{h,i}^0 = \mathcal{T}_{h,i}, \quad \mathcal{T}_{h,i}^\delta = \left\{K \in \mathcal{T}_h : \exists K' \in \mathcal{T}_{h,i}^{\delta-1}, \partial K' \cap \partial K \neq \emptyset\right\}.$$

Figure 4 shows an example of a non-overlapping and the corresponding overlapping partition obtained with METIS.[49] Now in the overlapping subdomains $\{\Omega_i^\delta\}_{i=1}^{np}$, we define local finite element subspaces

$$\boldsymbol{V}_h^i = \left\{\boldsymbol{v} \in \boldsymbol{V}_h\Big|_{\Omega_i^\delta} : \boldsymbol{v}\Big|_{\partial\Omega_i^\delta \setminus (\partial\Omega \setminus \Gamma_W)} = 0\right\}, Q_h^i = \left\{q \in Q_h\Big|_{\Omega_i^\delta} : q\Big|_{\partial\Omega_i^\delta \setminus \partial\Omega} = 0\right\}$$

and the natural restriction operator $R_i : \boldsymbol{V}_h \times Q_h \to \boldsymbol{V}_h^i \times Q_h^i$ which returns all degrees of freedom associated with the overlapping subdomains and $R_i^0 : \boldsymbol{V}_h \times Q_h \to \boldsymbol{V}_h^i \times Q_h^i$ which returns all degrees of freedom associated with the non-overlapping subdomains. The one-level restricted additive Schwarz preconditioner[50] can be defined as

$$M_{1s}^{-1} = \sum_{i=1}^{np} \left(R_i^0\right)^T A_i^{-1} R_i, \tag{17}$$

where $A_i = R_i A R_i^T$ is the ith subdomain matrix and A is the Jacobian matrix of (6) at each Newton step.

It is worth noting that the one-level preconditioner (17) only involves local information exchange between adjoining subdomains and the scalability is generally not guaranteed when the number of subdomains is large. Next, we introduce a two-level method by additively combining the one-level preconditioner with a coarse preconditioner to improve its scalability and robustness.

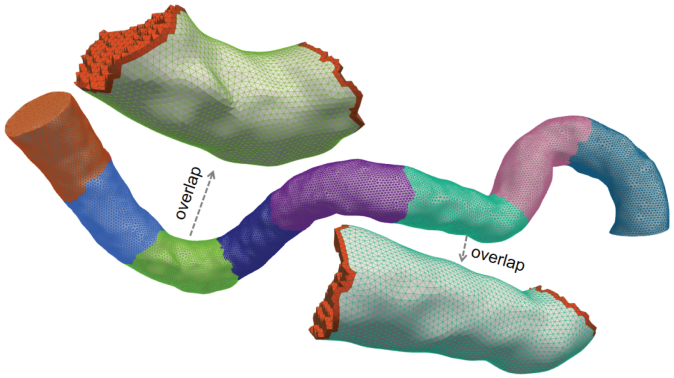

FIGURE 4 A non-overlapping partition of an arterial domain into 8 subdomains and the overlapping layers (red) are marked for two of the subdomains.

4.2 | Mixed-dimensional coarse preconditioner

In this subsection, we combine the discretization of the mixed-dimensional model given in Section 3 with suitable restriction and extension operators to construct a cheap and scalable coarse preconditioner. For simplicity, we ignore the superscript and denote $A_{mc}^{n,k}$ as A_{mc} in (16). Let $R_{mc}:\mathbb{R}^{4N}\to\mathbb{R}^{2N_{cl}^c+4N_a^c}$ and $E_{mc}:\mathbb{R}^{2N_{cl}^c+4N_a^c}\to\mathbb{R}^{4N}$ be the mixed-dimensional restriction and extension matrices, where N, N_{cl}^c and N_a^c are the numbers of mesh points of $\mathcal{T}_h, \mathcal{T}_H^{cl}$ and $\mathcal{T}_H^a$. Then the mixed-dimensional coarse preconditioner takes the form

$$M_{mc}^{-1}=E_{mc}A_{mc}^{-1}R_{mc}. \tag{18}$$

We first give some definitions and notations. Let $\{x_h^i\}_{i=1}^N$ be the collection of mesh points of $\mathcal{T}_h$ divided into two disjoint sets $\{x_{h,o}^i\}_{i=1}^{N_o}$ and $\{x_{h,a}^i\}_{i=1}^{N_a}$ in Ω_o and Ω_a, respectively, and $N=N_o+N_a$. Define $\boldsymbol{V}_h(\Omega_o)$ and $Q_h(\Omega_o)$ as the subspaces of $\boldsymbol{V}_h(\Omega)$ and $Q_h(\Omega)$ such that functions in $\boldsymbol{V}_h(\Omega_o)$ and $Q_h(\Omega_o)$ vanish at $\{x_{h,a}^i\}_{i=1}^{N_a}$, and similarly we define $\boldsymbol{V}_h(\Omega_a)$ and $Q_h(\Omega_a)$. Consequently we have $\boldsymbol{V}_h(\Omega)=\boldsymbol{V}_h(\Omega_o)\oplus\boldsymbol{V}_h(\Omega_a), Q_h(\Omega)=Q_h(\Omega_o)\oplus Q_h(\Omega_a)$. Next we define the extension and restriction matrices E_{mc} and R_{mc}.

First we define a restriction matrix $R_{o,cl}:\mathbb{R}^{4N_o}\to\mathbb{R}^{2N_{cl}^c}$ and an extension matrix $E_{o,cl}:\mathbb{R}^{2N_{cl}^c}\to\mathbb{R}^{4N_o}$ between the coarse finite element space $V_H^{cl}(\Omega_o^{cl})\times Q_H^{cl}(\Omega_o^{cl})$ and the fine finite element space $\boldsymbol{V}_h(\Omega_o)\times Q_h(\Omega_o)$, respectively. Let $\{s_i\}_{i=1}^{N_{cl}^c}$ be the collection of mesh points of $\mathcal{T}_H^{cl}$. Denote $\{I_i\}_{i=1}^{N_{cl}^c-1}$ as the collection of line elements of $\mathcal{T}_H^{cl}$. Then for any s in $\mathcal{T}_H^{cl}$, there exists a unique $j\in\{1,...,N_{cl}^c-1\}$, denoted by $j(s)$, such that $s\in I_j$. Define a mapping $\mathcal{I}:\{x_{h,o}^i\}_{i=1}^{N_o}\to\{I_i\}_{i=1}^{N_{cl}^c-1}$ by

$$\mathcal{I}\left(x_{h,o}^i\right)=I_j,$$

where $j=\min_{s\in s^*} j(s)$ and $s^*=\arg\min_{s\in\mathcal{T}_H^{cl}}\left|x_{h,o}^i-x(s)\right|$. Denote $\zeta(y)\,(y\in[0,1])$ as the interpolation function of the velocity on the normalized cross sections, which is defined as

$$\zeta(y)=\theta(1-y)+(1-\theta)\left(1-y^2\right),\theta\in\{0,1\}.$$

Note that ζ is linear when $\theta=1$ and quadratic when $\theta=0$ which is used in Reference 38. We define the extension operator from $\left(u_H^{cl},\ p_H^{cl}\right)\in V_H^{cl}(\Omega_o^{cl})\times Q_H^{cl}(\Omega_o^{cl})$ to $(\boldsymbol{u}_h,p_h)\in\boldsymbol{V}_h(\Omega_o)\times Q_h(\Omega_o)$ as

$$\boldsymbol{u}_h\left(x_{h,o}^j\right)=u_H^{cl}(s)\zeta\left(\frac{\left|x_{h,o}^j-x(s)\right|}{r_0(s)}\right)\tau(s),\quad p_h\left(x_{h,o}^j\right)=p_H^{cl}(s), \tag{19}$$

for any $x_{h,o}^j\ (j=1,...,N_o)$ with s satisfying $s\in\mathcal{I}\left(x_{h,o}^j\right)$ and $x_{h,o}^j\in C_s(s)$, where $\tau(s)$ is the unit tangential vector along the centerline. Denote $\{\varphi_i\}_{i=1}^{N_{cl}^c}$ as the nodal basis functions of $\mathcal{T}_H^{cl}$. Based on the definition (19), the extension matrix $E_{o,cl}:\mathbb{R}^{2N_{cl}^c}\to\mathbb{R}^{4N_o}$ can be given as[38]

$$E_{o,cl}=\begin{pmatrix} W_1^u & W_2^u & W_3^u & 0\\ 0 & 0 & 0 & W^p\end{pmatrix}^T, W_k^u=T_kW^u\,(k=1,2,3), \tag{20}$$

where $T_k=\operatorname{diag}\left(\tau^k(s_1),\cdots,\tau^k\left(s_{N_{cl}^c}\right)\right)$ are the tangent matrices and $W^l=\left(w_{ij}^l\right)_{N_{cl}^c\times N_o},(l=u,p)$ are the weighting matrices defined as

$$w_{ij}^u=\begin{cases}\zeta\left(\dfrac{r_j}{r_0}\right)\varphi_i(s), & x_{h,o}^j\in D_o^i, x_{h,o}^j\in C_s(s)\\ 0, & x_{h,o}^j\notin D_o^i\end{cases},\quad w_{ij}^p=\begin{cases}\varphi_i(s), & x_{h,o}^j\in D_o^i, x_{h,o}^j\in C_s(s)\\ 0, & x_{h,o}^j\notin D_o^i\end{cases},$$

with $D_o^i = \left\{ x \in \left\{ x_{h,o}^j \right\}_{j=1}^{N_o} : \mathcal{I}(x) \subset [s_{i-1}, s_{i+1}], x \in C_s(s), \forall s \in [s_{i-1}, s_{i+1}] \right\}$. The restriction matrix $R_{o,cl}$ is defined as the transpose of $E_{o,cl}$.

Then we define a restriction matrix $R_{a,c} : \mathbb{R}^{4N_a} \to \mathbb{R}^{4N_a^c}$ and an extension matrix $E_{a,c} : \mathbb{R}^{4N_a^c} \to \mathbb{R}^{4N_a}$ between the coarse finite element space $\boldsymbol{V}_H^a(\Omega_a) \times Q_H^a(\Omega_a)$ and the fine finite element space $\boldsymbol{V}_h(\Omega_a) \times Q_h(\Omega_a)$. Let $\left\{ x_{H,a}^i \right\}_{i=1}^{N_a^c}$ be the collection of mesh points of $\mathcal{T}_H^a$. Following,[3,51] using radial basis functions (RBF) denoted $\phi(r, \varepsilon)$ (see Table 1) with the rescaled technique,[51] the extension operator from $(\boldsymbol{u}_H, p_H) \in \boldsymbol{V}_H^a(\Omega_a) \times Q_H^a(\Omega_a)$ to $(\boldsymbol{u}_h, p_h) \in \boldsymbol{V}_h(\Omega_a) \times Q_h(\Omega_a)$ can be defined as

$$Z_h\left(x_{h,a}^i\right) = \sum_{x_{H,a}^j \in D_H^i} w_{ij} Z_H\left(x_{H,a}^j\right), w_{ij} = \frac{\widetilde{w}_{ij}}{\sum_{x_{H,a}^k \in D_H^i} \widetilde{w}_{ik}}, \widetilde{w}_i = \Phi^{-1} \phi_i, (Z = \boldsymbol{u}, p) \tag{21}$$

with the vectors $\widetilde{w}_i = (w_{ij}), \phi_i = \left(\phi_{ij}\right)$ for any $x_{h,a}^i$ $(i = 1, ..., N_a)$, where $\phi_{ij} = \phi\left(r_{ij}, 1/H_i\right)$, Φ is the interpolate matrix with elements ϕ_{jk}, $r_{ij} = | x_{h,a}^i - x_{H,a}^j |$, H_i is the diameter of D_H^i and D_H^i is the collection of the first four coarse mesh points of $\mathcal{T}_H^a$ close to $x_{h,a}^i$. Through numerical experiments, we find that if Φ is replaced by the identify matrix the performance of the algorithm is actually better in the sense that the number of iterations is smaller without having any accuracy issue. In this case, the weight w_{ij} reduces to

$$w_{ij} = \frac{\phi\left(r_{ij}, 1/H_i\right)}{\sum_{x_{H,a}^k \in D_H^i} \phi(r_{ik}, 1/H_i)}. \tag{22}$$

By the definition of the extension operator in (21), the extension matrix $E_{a,c} : \mathbb{R}^{4N_a^c} \to \mathbb{R}^{4N_a}$ is stated as

$$E_{a,c} = \operatorname{diag}\left(E_{rbf}, E_{rbf}, E_{rbf}, E_{rbf}\right), E_{rbf} = \left(e_{ij}\right)_{N_a \times N_a^c}, e_{ij} = \begin{cases} w_{ij} & x_{H,a}^j \in D_H^i \\ 0 & x_{H,a}^j \notin D_H^i \end{cases}. \tag{23}$$

Similarly, the restriction matrix $R_{a,c}$ is defined as the transpose of $E_{a,c}$.

Finally, using $E_{o,cl}$ defined in (20) and $E_{a,c}$ defined in (23), the mixed-dimensional extension matrix $E_{mc} : \mathbb{R}^{2N_{cl}^c + 4N_a^c} \to \mathbb{R}^{4N}$ can be obtained by

$$E_{mc} = \begin{pmatrix} E_{o,cl} & 0 \\ 0 & E_{a,c} \end{pmatrix} \tag{24}$$

TABLE 1 Common radial basis functions.

Type	RBF
Local compact support (CP2)	$(1 - \varepsilon r)^4 (1 + 4\varepsilon r)$
Polyharmonic spline (PHS(m))	$r^m (m = 1, 3, ...); r^m \log(r) (m = 2, 4, ...)$
Multiquadric biharmonic (MQB)	$\sqrt{1 + (\varepsilon r)^2}$
Inverse quadratic (IQ)	$1/\left(1 + (\varepsilon r)^2\right)$
Inverse multiquadric (IMQ)	$1/\sqrt{1 + (\varepsilon r)^2}$
Gaussian (GA)	$e^{-(\varepsilon r)^2}$

and the corresponding restriction matrix R_{mc} is given as the transpose of E_{mc}. Consequently combining the one-level preconditioner (17) with the coarse preconditioner (18), we obtain a mixed-dimensional two-level additive Schwarz preconditioner

$$M_{2s,mc}^{-1} = M_{mc}^{-1} + M_{1s}^{-1} = E_{mc} A_{mc}^{-1} R_{mc} + \sum_{i=1}^{np} \left(R_i^0\right)^T A_i^{-1} R_i. \tag{25}$$

For the following numerical comparison, we also consider a full 1D coarse preconditioner M_{cl}^{-1} defined on the entire central-line coarse mesh (see the left subfigure of Figure 5) and a full 3D coarse preconditioner M_c^{-1} defined on the whole 3D coarse mesh (see the right subfigure of Figure 5). The full 1D and 3D coarse preconditioners can be obtained similarly to the 1D and 3D parts of the mixed-dimensional coarse preconditioner, respectively. The corresponding two-level preconditioners are denoted by $M_{2s,cl}^{-1}$ and $M_{2s,c}^{-1}$.

Remark 1. The aforementioned coarse preconditioners rely on the coarse solution at the current Newton step when $\beta = 1$. In order to obtain the coarse solutions, we restrict the current Newton solution from the fine finite element space into the coarse finite element space using radial basis functions. Specifically for the mixed-dimensional coarse preconditioner, given the current Newton solution $(\boldsymbol{u}_h, p_h)$ and the radial basis functions $\phi(r,\varepsilon)$, the coarse solution $\left(u_H^{cl}, p_H^{cl}, \boldsymbol{u}_H, p_H\right)$ can be obtained by the following restriction operations

$$u_H^{cl}(s_i) = \sum_{x_{h,o}^j \in D_{h,o}^i} w_{ij}^o \boldsymbol{u}_h\left(x_{h,o}^j\right) \tau(s_i), p_H^{cl}(s_i) = \sum_{x_{h,o}^j \in D_{h,o}^i} w_{ij}^o p_h\left(x_{h,o}^j\right), \tag{26}$$

$$\boldsymbol{u}_H\left(x_{H,a}^i\right) = \sum_{x_{h,a}^j \in D_{h,a}^i} w_{ij}^a \boldsymbol{u}_h\left(x_{h,a}^j\right), p_H\left(x_{H,a}^i\right) = \sum_{x_{h,a}^j \in D_{h,a}^i} w_{ij}^a p_h\left(x_{h,a}^j\right), \tag{27}$$

where the weights $w_{ij}^l\,(l = o, a)$ can be obtained similarly to (21).

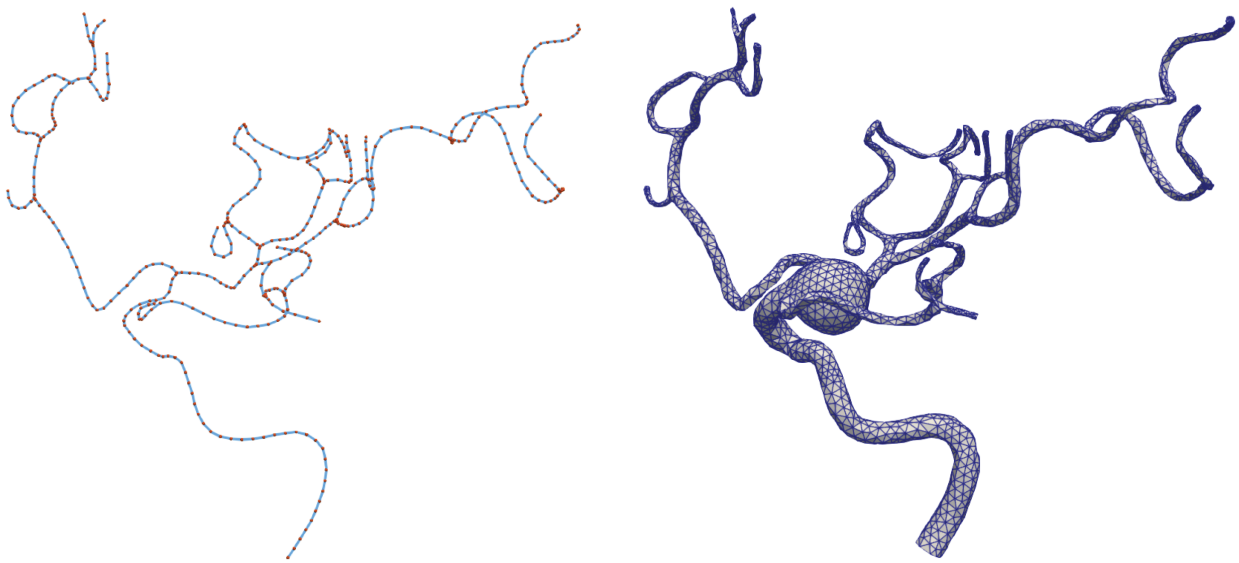

FIGURE 5 A full central-line mesh (left) with about 4×10^2 mesh points and a full 3D coarse mesh (right) with about 4×10^3 mesh points of an aneurysmal artery.

5 | A MIXED-DIMENSIONAL COARSE CORRECTION OF THE INITIAL GUESS FOR INEXACT NEWTON

The nonlinear system (6) is solved by an inexact Newton method whose convergence depends on a good initial guess which is often not available. In this section, we introduce a good initial guess for the first time step using the mixed-dimensional coarse preconditioner defined in (18). For simplicity, we denote the nonlinear system at the current time step as $F(x)=0$, and a mixed-dimensional coarse correction function $\mathcal{C}_{mc}:\mathbb{R}^{4N}\to\mathbb{R}^{4N}$ is as

$$\mathcal{C}_{mc}(x)=x-\lambda_{mc}M_{mc}^{-1}F(x),\quad \forall x\in\mathbb{R}^{4N}, \tag{28}$$

where $\lambda_{mc}\in(0,1]$ is a step-size parameter. Note that $\mathcal{C}_{mc}(x)=x$ if and only if x is a root of F. The correction takes the following steps:

1. compute the nonlinear residual: $F(x_k)$.
2. obtain the 3D correction, specifically
   - compute the mixed-dimensional residual by restriction: $F_{mc}(x_k)=R_{mc}F(x_k)$.
   - compute the correction by solving the mixed-dimensional residual equations: $A_{mc}\delta_{mc}^{k}=F_{mc}(x_k)$.
   - compute the 3D correction by extension: $\delta_k=E_{mc}\delta_{mc}^{k}$.
3. correct the solution: $\mathcal{C}_{mc}(x_k)=x_k-\lambda_{mc}\delta_k$.

We remark that the coarse correction has two advantages: it is cheap and it saves a lot of Newton iterations.

Finally, a Newton-Krylov method with the mixed-dimensional coarse preconditioner and initial guess correction for solving (6) can be described in Algorithm 1, in which the step-size parameter $\lambda_{mc}=1$, the Jacobian matrix J_k^n of F^n at

Algorithm 1 **Newton-Krylov method with mixed-dimensional coarse correction of the initial guess for $\boldsymbol{F^n(X^n)=0}$**

1: Given an initial guess $X_0^n=X^{n-1}$.
2: Correct the initial guess $\widehat{X}_0^n=\mathcal{C}_{mc}(X_0^n)$ and reset $X_0^n=\widehat{X}_0^n$ when $n=1$.
3: **for** $k=0,1,2,\ldots$ **do**
4: Find the Newton direction s_k^n by approximately solving the Jacobian system by a preconditioned GMRES method

$$J_k^n\left(M_{2s,mc}^{n,k}\right)^{-1}M_{2s,mc}^{n,k}s_k^n=-F^n\left(X_k^n\right), \tag{29}$$

with the stopping condition

$$\left\|F^n\left(X_k^n\right)+J_k^ns_k^n\right\|_2\le\max\left\{atol_{\text{GMRES}},rtol_{\text{GMRES}}\left\|F^n\left(X_k^n\right)\right\|_2\right\}. \tag{30}$$

5: Find the step length λ_k^n by the line search technique

$$f\left(X_k^n+\lambda_k^ns_k^n\right)\le f\left(X_k^n\right)+\varepsilon\lambda_k^n\nabla f\left(X_k^n\right)^Ts_k^n. \tag{31}$$

6: Update the Newton solution $X_{k+1}^n=X_k^n+\lambda_k^ns_k^n$.
7: **if** $\left\|F^n\left(X_{k+1}^n\right)\right\|_2\le\max\left\{atol_{\text{Newton}},rtol_{\text{Newton}}\left\|F^n\left(X_0^n\right)\right\|_2\right\}$ **then**
8: $X^n=X_{k+1}^n$, return.
9: **end if**
10: **end for.**

X_k^n is analytically calculated, $\left(M_{2s,mc}^{n,k}\right)^{-1}$ is the proposed two-level Schwarz preconditioner at X_k^n, f is a merit function defined as $f(X) = \|F(X)\|_2^2/2$ and the linesearch parameter $\varepsilon = 10^{-4}$. The absolute and relative tolerances $atol_{\text{GMRES}}, rtol_{\text{GMRES}}$ and $atol_{\text{Newton}}, rtol_{\text{Newton}}$ are used to control the Krylov and Newton iterations, respectively.

6 | NUMERICAL EXPERIMENTS

Some numerical experiments are provided in this section to show the effectiveness of the proposed mixed-dimensional coarse preconditioner and correction for unsteady incompressible Navier–Stokes flows in a 3D patient-specific aneurysmal artery including one inlet and fifteen outlets. The diameters of inlet and outlets of the artery are about 6 mm and 1.2 mm. For the blood flows, we set the viscosity $\nu = 0.035$ g/(cm·s), the density $\rho = 1$ g/cm^3. On the inlet, we prescribe a pulsatile periodic flow velocity[3] (see Figure 6) with a parabolic profile. On each outlet Γ_O^i, the resistance $R_O^i = R_{total} \sum_{j=1}^m \left|\Gamma_O^j\right|^{1.5} / \left|\Gamma_O^i\right|^{1.5}$ with $R_{total} = 1500$ dyn·s/cm^5. Here the value of the resistance is from Reference 38 In Algorithm 1, we set $rtol_{\text{Newton}} = 10^{-4}, atol_{\text{Newton}} = 10^{-6}$ and $rtol_{\text{GMRES}} = 10^{-4}, atol_{\text{GMRES}} = 10^{-6}$. The linear Jacobian system at each Newton step is solved by the right-preconditioned GMRES (30). In the Schwarz preconditioner, we set the overlapping parameter $\delta = 1$, the subdomain problems is solved by incomplete LU (ILU) method with one fill-in level and the coarse problem is solved by direct method. Several different meshes are considered and their details are listed in Table. 2.

We consider the blood flow in a patient-specific cerebral artery depicted in Figure 2 (left) with the aneurysm marked in red. By solving (6) on a mesh with 2,789,226 elements and $\Delta t = .005$s, we obtain the numerical solution for a cardiac cycle. Figure 7 shows the computed streamlines and wall shear stress at the peak systole ($t = .165$s) and a diastole stage ($t = .4$s). We observe that the fluid flows along the centerline of the normal region and recirculates in the aneurysmal region, and the wall shear stress in the aneurysmal region is lower than that in the normal region, which is consistent with the results in Reference 2, indicating that the low wall shear stress might be a factor for the growth of the aneurysm and might lead to the localized degeneration of the aneurysmal wall. Figure 8 shows more details of the local features of the aneurysm including the streamline, the distribution of the magnitude of the velocity, and the wall shear

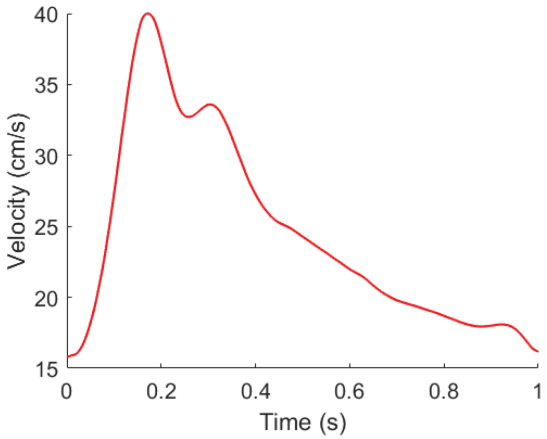

FIGURE 6 Inflow velocity for a cardiac cycle.

TABLE 2 Information of some 3D fine meshes and mixed-dimensional coarse meshes to be used in the experiments.

3D fine meshes			Mixed-dimensional coarse meshes			
N	E	h (mm)	N_{cl}^c	H_{cl} (mm)	N_a^c	H_a (mm)
597,556	2,789,226	.22	297	2.61	109	3.00
1,582,006	8,738,883	.17	420	1.85	210	2.30
			784	1.00	350	1.80

Note: N, E, and h denote the number of mesh points, the number of elements and the mesh size. N_{cl}^c and H_{cl} denote the number of mesh points and the mesh size on the centerline, and N_a^c and H_a denote the number of mesh points and the mesh size in the aneurysmal region.

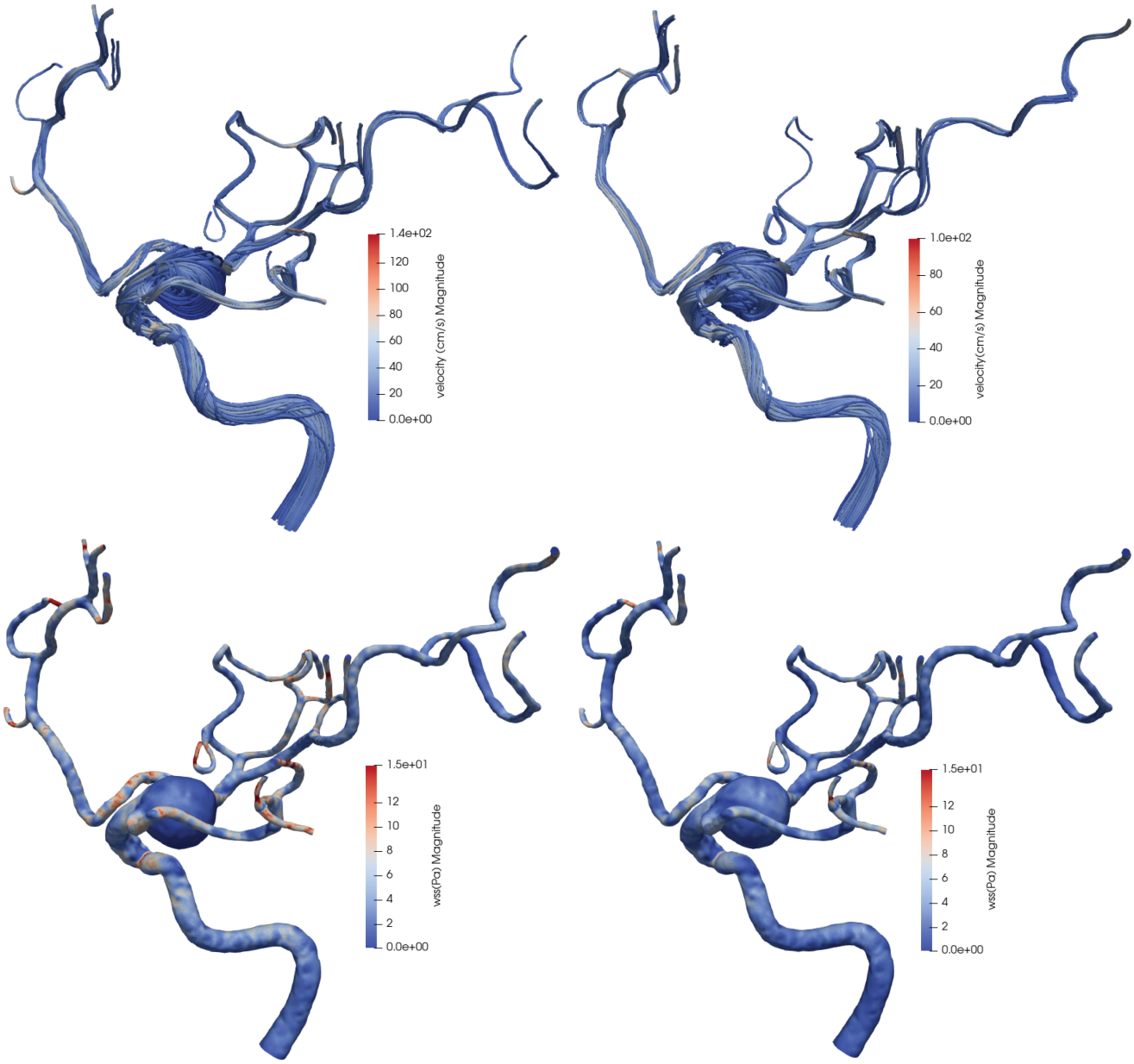

FIGURE 7 Distributions of streamlines (top) and wall shear stresses (bottom) at $t = .165$s (left) and $t = .4$s (right).

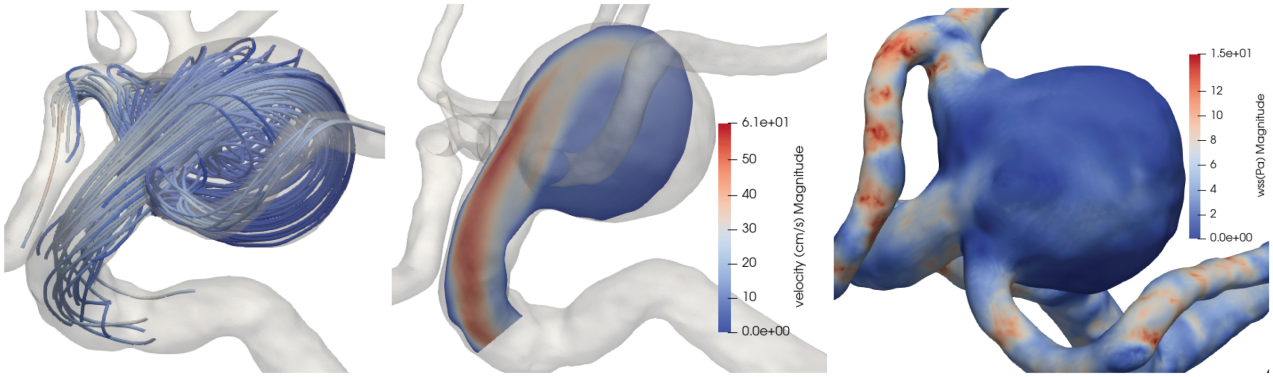

FIGURE 8 Local features of the streamline (left), the magnitude of a cross-sectional velocity (middle) and the wall shear stress (right) in the aneurysmal region at $t = .165$s.

stress. We see that a single vortex is formed within the aneurysmal region, which is reasonable as the inflow jet flows against the aneurysmal wall. Besides, the magnitudes of the wall shear stress at the neck and downstream lips of the aneurysm are significantly higher than that in the aneurysm and the inflow jet does not produce an obvious impingement zone and local elevation of the wall shear stress, which might mean a lower probability of rupture.[1]

6.1 | Performance of 1D coarse preconditioner without aneurysm

We first consider the artery shown in Figure 2 (left), but with the aneurysm removed (see Figure 9). This is an easier situation and we investigate the performance of the 1D coarse preconditioner. The 1D preconditioner $M_{cl}^{-1}(\theta,\eta)$ given in the paper is more general than the 1D preconditioner introduced in.[38] As discussed before, θ is a positive parameter imposed on the momentum equation of 1D Navier–Stokes equations, and η is an interpolation parameter. In this experiment, the time step size $\Delta t = .005$s, the fine mesh has 536,890 points and 2,497,260 elements and the central-line coarse mesh has 297 points. Table 3 shows the numbers of Newton and GMRES iterations with different values of θ,η and γ. Figure 9 shows the corresponding pressure distribution at $t = .05$s. We can see that the linear function ($\theta = 1$) as the velocity profile in the restriction and extension matrices gives a more effective 1D preconditioner than the quadratic function ($\theta = 0$), and a careful choice of η and γ can reduce the number of GMRES iterations. Usually, we set $\eta = 1$ and $\gamma = .05$, but the optimal values of the parameters are obtained experimentally. In the rest of the paper, we fix $\theta = 1$ and $\eta = 7$. This example shows that the 1D coarse preconditioner with appropriate parameters works well in complex

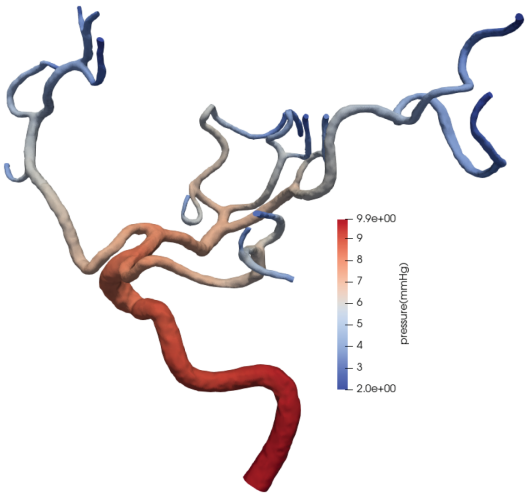

FIGURE 9 Computed pressure field in the artery without aneurysm at $t = .05$s.

TABLE 3 Effect of some parameters on the numbers of Newton and GMRES iterations of 1D coarse preconditioner ($\beta = 0$) for the artery without aneurysm at the tenth time step ($t = .05$s).

θ	η	γ	Newton	GMRES
0	1	.05	2	169.00
0	1	.15	2	160.00
0	1	.30	2	223.00
1	1	.05	2	110.50
1	1	.15	2	105.00
1	1	.30	2	124.50
1	3	.15	2	86.00
1	5	.15	2	71.50
1	7	.15	2	66.50

TABLE 4 Performance of the mixed-dimensional coarse correction at the first time step.

N	Δt (s)	*cor*	Newton	GMRES
597,556	.005	0	16	93.38
		1	4	56.00
	.01	0	16	95.88
		1	5	59.00
1,582,006	.005	0	11	107.64
		1	4	62.50
	.01	0	11	103.36
		1	4	75.00

Note: *cor* = 0 or 1 means the correction option is off and on, respectively.

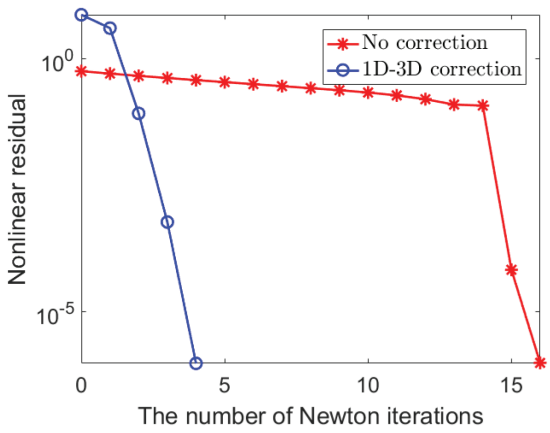

FIGURE 10 Nonlinear residual histories with and without mixed-dimensional coarse correction.

arteries without aneurysms. Next, we show the degradation of the performance of the 1D coarse preconditioner when there is an aneurysm and how the addition of the 3D coarse preconditioner in the aneurysmal region improves the performance.

6.2 | Performance of mixed-dimensional coarse preconditioner and initial-guess correction

In this subsection, we study the performance of the mixed-dimensional coarse preconditioner and the initial guess correction for the problem with an aneurysm as shown in Figure 2 (left). In Table 4, we show the numbers of Newton and GMRES iterations for two different mesh sizes and different time step sizes with and without mixed-dimensional coarse correction at the first time step. It is clear that both numbers of Newton and GMRES decrease significantly when the initial guess correction is used. Figure 10 shows the history of the nonlinear residual with and without the initial-guess correction, and it is clear that the correction is quite effective.

In Table 5, we show the numbers of Newton and GMRES iterations with a fixed $\Delta t = .005$s, and varying some of the parameters including the coarse mesh size, the type of the coarse model, the radial basis function, and the stabilization parameter. From this table, we observe that different radial basis functions do not affect the preconditioner, the coarse Navier–Stokes model ($\beta = 1$) is more effective than the coarse Stokes model ($\beta = 0$) and a suitable stabilization parameter $\gamma = .7$ can clearly reduce the number of GMRES iterations. In addition, we note that the number of GMRES iterations does not decrease when the number of coarse mesh points increases beyond a certain value. In other words, the coarse mesh does not need to be too fine.

TABLE 5 Effect of parameters on the numbers of Newton and GMRES iterations with mixed-dimensional coarse preconditioner at the tenth time step.

N_{cl}^c	N_a^c	β	RBF	γ	Newton	GMRES
784	109	0	CP2	.05	2	88.50
784	109	0	CP2	.7	2	82.50
784	109	0	CP2	1.2	2	82.00
784	109	0	GA	.7	2	82.50
784	109	0	MQB	.7	2	82.50
784	109	1	MQB	.7	2	76.50
784	210	1	MQB	.7	2	81.50
784	350	1	MQB	.7	2	104.00
420	109	1	MQB	.7	2	82.50
297	109	1	MQB	.7	2	78.50

Note: N_{cl}, N_a^c are the numbers of mesh points on the centerline and aneurysmal region, β is the model parameter, γ is the stabilization parameter, and "RBF" is the type of radial basis functions.

TABLE 6 Comparison of one-level and proposed two-level preconditioners with different numbers of mesh points N and different number of subdomains np at the peak systole.

		One-level		Two-level	
N	np	Newton	GMRES	Newton	GMRES
597,556	128	2	389.50	2	63.50
	256	2	419.50	2	66.00
	512	2	460.00	2	69.00
1,582,006	256	3	600.00	3	89.33
	512	3	600.00	3	92.00
	1024	3	600.00	3	94.00

Note: The maximum number of GMRES iterations is set to 600.

Next, we compare the scalability and effectiveness of the one-level and two-level preconditioners. Table 6 shows the numbers of Newton and GMRES iterations for different mesh sizes and number of subdomains at the peak systole. It can be seen that the number of GMRES iterations of the two-level preconditioner is far fewer than that of the one-level preconditioner, and it increases moderately when the mesh is refined and slightly when the number of subdomains increases. Figure 11 further presents the histories of the GMRES residuals of these preconditioners at the first two Newton steps. Note that the GMRES residual decreases fast and almost linearly for the two-level preconditioner but slowly for the one-level preconditioner after some iterations.

Finally, we consider the performance of the mixed-dimensional coarse preconditioner compared with 1D and 3D coarse preconditioners. Table 7 shows the numbers of Newton and GMRES iterations of these preconditioners with Stokes or Navier–Stokes model at the peak systole. For the 3D and mixed-dimensional preconditioners, the Navier–Stokes coarse model ($\beta = 1$) can significantly reduce the number of GMRES iterations of the Stokes coarse model ($\beta = 0$). The full 1D coarse preconditioner performs badly, however, the mixed-dimensional coarse preconditioner, which is obtained by replacing the aneurysmal part of the full 1D coarse preconditioner with a 3D coarse preconditioner in the aneurysmal region, has a significant improvement and is comparable to the 3D preconditioner when $\beta = 1$. Figure 12 shows the sparsity patterns and the number of nonzero elements of these coarse matrices. It is easy to see that the mixed-dimensional coarse matrix has a local denser submatrix than the full 1D coarse matrix, and they have far fewer non-zeros than the 3D coarse matrix. These results indicate that for the aneurysmal artery the mixed-dimensional coarse preconditioner not only performs well in terms of the number of GMRES iterations but also has only a small increase in the dimension and the density compared with the 1D coarse preconditioner (Figure 12).

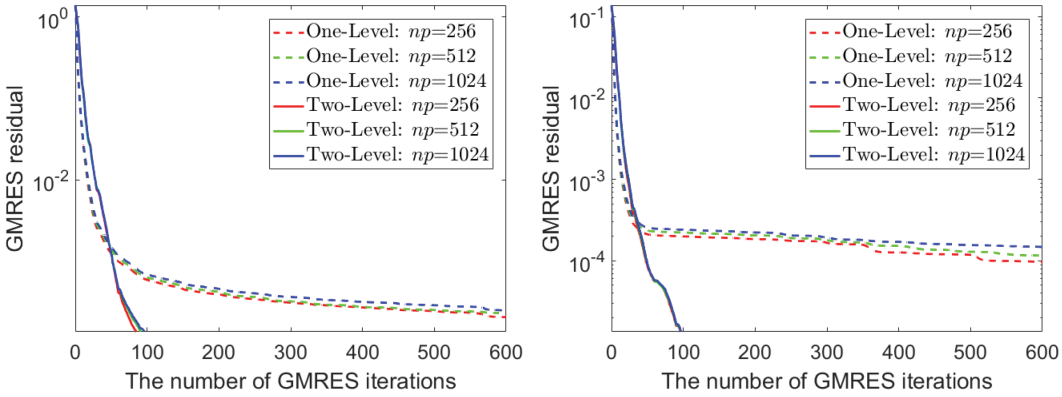

FIGURE 11 GMRES residual histories of the one-level and two-level preconditioners at the first (left) and second (right) Newton steps with $N = 1582006$ at the peak systole.

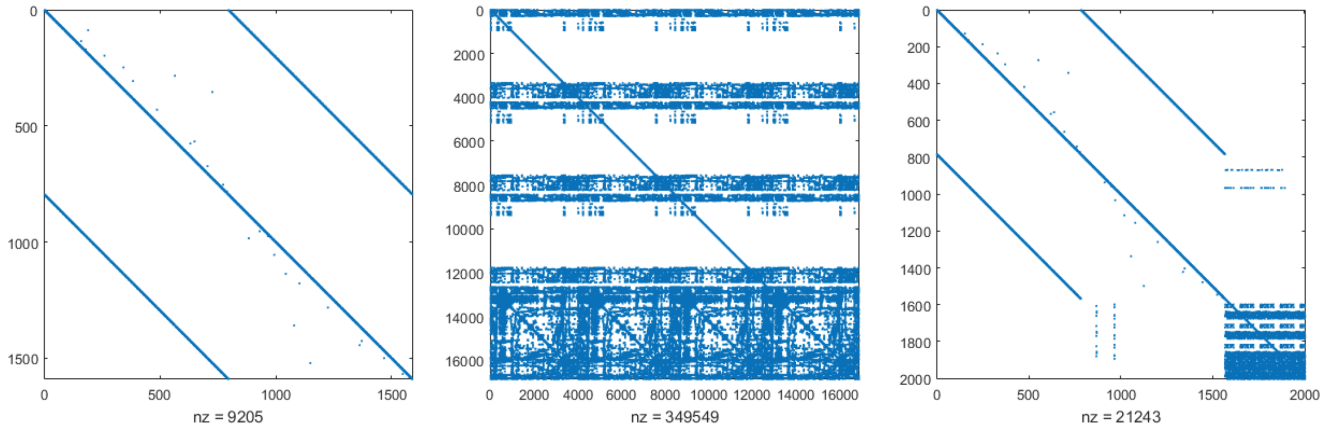

FIGURE 12 Sparsity pattern of 1D (left), 3D (middle) and mixed-dimensional (right) coarse matrices with $\beta = 1$.

TABLE 7 Comparison of the 1D, 3D, and mixed-dimensional (mD) coarse preconditioners at the peak systole.

Preconditioner	Dim	*nnz*	β	RBF	γ	Newton	GMRES
1D	1590	9205	0	-	.7	2	237.50
1D		9205	1	MQB	.7	2	236.00
3D	16,872	269,947	0	CP2	7.0	2	223.50
3D		349,549	1	CP2	7.0	2	68.00
mD	2004	17,746	0	MQB	.7	2	92.50
mD		21,243	1	MQB	.7	2	63.50

Note: "Dim" is the dimension of the coarse matrix, *nnz* is the number of nonzeros in the coarse matrix, β is the model parameter and γ is the stabilization parameter.

7 | CONCLUSIONS

High-fidelity simulation of 3D unsteady incompressible Navier–Stokes equations is becoming an important tool to understand the behavior of the blood flows in the human artery, but the simulation is computationally expensive, especially when there is aneurysm since the fluid becomes much more complex. In this paper, we develop and test a Newton-Krylov method with a two-level additive Schwarz preconditioner with a mixed-dimensional coarse space and also a mixed-

dimensional initial guess correction for solving the 3D Navier–Stokes equations. In the two-level preconditioner, we construct an effective and scalable coarse preconditioner by combining a 1D coarse preconditioner defined on the centerline of the normal region and a 3D coarse preconditioner defined in the aneurysmal region. Such a mixed-dimensional coarse preconditioner is later modified to provide an initial guess correction for the inexact Newton's method for the first time step. For a patient-specific cerebral flow problem, we show numerically that the proposed methods reduce the numbers of the linear and nonlinear iterations significantly while keeping a very low computational complexity.

ACKNOWLEDGEMENTS

The research was supported by the NSFC through Grant 12201658 and the FDCT through Grant 0141/2021/A3, 0079/2021/AFJ.

DATA AVAILABILITY STATEMENT

The data that support the findings of the study are available from the corresponding author upon reasonable request.

ORCID

Yingzhi Liu https://orcid.org/0000-0001-9962-7310

REFERENCES

1. Sforza DM, Putman CM, Cebral JR. Hemodynamics of cerebral aneurysms. *Annu Rev Fluid Mech*. 2009;41:91-107.
2. Shojima M, Oshima M, Takagi K, et al. Magnitude and role of wall shear stress on cerebral aneurysm: computational fluid dynamic study of 20 middle cerebral artery aneurysms. *Stroke*. 2004;35(11):2500-2505.
3. Chen R, Wu B, Cheng Z, et al. A parallel non-nested two-level domain decomposition method for simulating blood flows in cerebral artery of stroke patient. *Int J Numer Meth Biomed Engng*. 2020;36(11):e3392.
4. Kong F, Kheyfets V, Finol E, Cai XC. An efficient parallel simulation of unsteady blood flows in patient-specific pulmonary artery. *Int J Numer Meth Biomed Engng* 2018; 34(4): e2952.
5. Lin Z, Chen R, Gao B, et al. A highly parallel simulation of patient-specific hepatic flows. *Int J Numer Meth Biomed Engng* 2021; 37(6): e3451.
6. Qin S, Wu B, Liu J, et al. Numerical simulation of blood flows in patient-specific abdominal aorta with primary organs. *Biomech Model Mechanobiol*. 2021;20:909-924.
7. Quarteroni A, Manzoni A, Vergara C. The cardiovascular system: mathematical modelling, numerical algorithms and clinical applications. *Acta Numer*. 2017;26:365-590.
8. Quarteroni A, Tuveri M, Veneziani A. Computational vascular fluid dynamics: problems, models and methods. *Comput Vis Sci*. 2000; 2(4):163-197.
9. Taylor CA, Fonte TA, Min JK. Computational fluid dynamics applied to cardiac computed tomography for noninvasive quantification of fractional flow reserve: scientific basis. *J Am Coll Cardiol*. 2013;61(22):2233-2241.
10. Taylor CA, Hughes TJ, Zarins CK. Finite element modeling of blood flow in arteries. *Comput Methods Appl Mech Eng*. 1998;158(1–2): 155-196.
11. Grinberg L, Karniadakis GE. Outflow boundary conditions for arterial networks with multiple outlets. *Ann Biomed Eng*. 2008;36(9): 1496-1514.
12. Olufsen MS. Structured tree outflow condition for blood flow in larger systemic arteries. *Am J Physiol Heart Circ Physiol*. 1999;276(1): H257-H268.
13. Vignon-Clementel IE, Figueroa CA, Jansen KE, Taylor CA. Outflow boundary conditions for three-dimensional finite element modeling of blood flow and pressure in arteries. *Comput Methods Appl Mech Eng*. 2006;195(29–32):3776-3796.
14. Knoll DA, Keyes DE. Jacobian-free Newton-Krylov methods: a survey of approaches and applications. *J Comput Phys*. 2004;193(2): 357-397.
15. Dennis JE, Schnabel RB. *Numerical Methods for Unconstrained Optimization and Nonlinear Equations*. SIAM; 1996.
16. Saad Y. *Iterative Method for Sparse Linear Systems*. second ed. SIAM; 2003.
17. Klawonn A. An optimal preconditioner for a class of saddle point problems with a penalty term. *SIAM J Sci Comput*. 1998;19(2):540-552.
18. Klawonn A. Block-triangular preconditioners for saddle point problems with a penalty term. *SIAM J Sci Comput*. 1998;19(1):172-184.
19. Quarteroni A, Saleri F, Veneziani A. Analysis of the Yosida method for the incompressible Navier-Stokes equations. *J Math Pures Appl*. 1999;78(5):473-503.
20. Quarteroni A, Saleri F, Veneziani A. Factorization methods for the numerical approximation of Navier-Stokes equations. *Comput Methods Appl Mech Eng*. 2000;188(1–3):505-526.
21. Elman H, Howle VE, Shadid J, Shuttleworth R, Tuminaro R. A taxonomy and comparison of parallel block multi-level preconditioners for the incompressible Navier-Stokes equations. *J Comput Phys*. 2008;227(3):1790-1808.
22. Elman H, Howle VE, Shadid J, Silvester D, Tuminaro R. Least squares preconditioners for stabilized discretizations of the Navier-Stokes equations. *SIAM J Sci Comput* 2007 30(1): 290–311.

23. Silvester D, Elman H, Kay D, Wathen A. Efficient preconditioning of the linearized Navier-Stokes equations for incompressible flow. *J Comput Appl Math*. 2001;128(1–2):261-279.
24. Benzi M, Guo XP. A dimensional split preconditioner for Stokes and linearized Navier-Stokes equations. *Appl Numer Math*. 2011;61(1):66-76.
25. Benzi M, Ng M, Niu Q, Wang Z. A relaxed dimensional factorization preconditioner for the incompressible Navier-Stokes equations. *J Comput Phys*. 2011;230(16):6185-6202.
26. Balzani D, Böse D, Brands D, et al. Parallel simulation of patient-specific atherosclerotic arteries for the enhancement of intravascular ultrasound diagnostics. *Eng Comput*. 2012;29(8):888-906.
27. Li J, Widlund O. BDDC algorithms for incompressible Stokes equations. *SIAM J Numer Anal*. 2006;44(6):2432-2455.
28. Heinlein A, Hochmuth C, Klawonn A. Monolithic overlapping Schwarz domain decomposition methods with GDSW coarse spaces for incompressible fluid flow problems. *SIAM J Sci Comput*. 2019;41(4):C291-C316.
29. Klawonn A, Pavarino LF. Overlapping Schwarz methods for mixed linear elasticity and Stokes problems. *Comput Methods Appl Mech Eng*. 1998;165(1–4):233-245.
30. Kong F, Cai XC. A highly scalable multilevel Schwarz method with boundary geometry preserving coarse spaces for 3D elasticity problems on domains with complex geometry. *SIAM J Sci Comput*. 2016;38(2):C73-C95.
31. Gee MW, Küttler U, Wall WA. Truly monolithic algebraic multigrid for fluid-structure interaction. *Int J Numer Methods Eng*. 2011;85(8):987-1016.
32. Randles A, Draeger EW, Oppelstrup T, Krauss L, Gunnels JA. Massively parallel models of the human circulatory system. *SC '15*. Association for Computing Machinery; 2015:1-11.
33. Zhang Y, Bazilevs Y, Goswami S, Bajaj CL, Hughes TJ. Patient-specific vascular NURBS modeling for isogeometric analysis of blood flow. *Comput Methods Appl Mech Eng*. 2007;196(29):2943-2959.
34. Smith B, Bjørstad PE, Gropp W. *Domain Decomposition: Parallel Multilevel Methods for Elliptic Partial Differential Equations*. Cambridge University Press; 1996.
35. Toselli A, Widlund O. *Domain Decomposition Methods–Algorithms and Theory*. Springer-Verlag; 2005.
36. Liu Y, Cai XC. A central-line coarse preconditioner for Stokes flows in artery-like domains. *Numer Algorithms*. 2021;87(1):137-160.
37. Liu Y, Cai XC. Two-level additive Schwarz methods for three-dimensional unsteady Stokes flows in patient-specific arteries with parameterized one-dimensional central-line coarse preconditioner. *J Comput Phys*. 2023;490:112290.
38. Liu Y, Qi F, Cai XC. A one-dimensional coarse preconditioner for three-dimensional unsteady incompressible Navier-Stokes flows in patient-specific arteries. *SIAM J Sci Comput*. 2022;S1-S23.
39. Formaggia L, Gerbeau JF, Nobile F, Quarteroni A. On the coupling of 3D and 1D Navier–Stokes equations for flow problems in compliant vessels. *Comput Methods Appl Mech Eng*. 2001;191(6–7):561-582.
40. Formaggia L, Lamponi D, Quarteroni A. One-dimensional models for blood flow in arteries. *J Eng Math*. 2003;47(3–4):251-276.
41. Quarteroni A, Formaggia L. Mathematical modelling and numerical simulation of the cardiovascular system. *Handb Numer Anal*. 2004;12:3-127.
42. Reymond P, Merenda F, Perren F, Rufenacht D, Stergiopulos N. Validation of a one-dimensional model of the systemic arterial tree. *Am J Physiol Heart Circ Physiol*. 2009;297(1):H208-H222.
43. Sherwin S, Franke V, Peiro J, Parker K. One-dimensional modelling of a vascular network in space-time variables. *J Eng Math*. 2003;47(3–4):217-250.
44. Smith N, Pullan A, Hunter P. An anatomically based model of transient coronary blood flow in the heart. *SIAM J Appl Math*. 2002;62(3):990-1018.
45. Boffi D, Brezzi F, Fortin M. Mixed finite element methods and applications. *44 of Springer Series in Computational Mathematics*. Springer; 2013.
46. Franca LP, Frey SL. Stabilized finite element methods. II. The incompressible Navier-Stokes equations. *Comput Methods Appl Mech Eng* 1992; 99: 209–233, 233.
47. Formaggia L, Gerbeau JF, Nobile F, Quarteroni A. Numerical treatment of defective boundary conditions for the Navier-Stokes equations. *SIAM J Numer Anal*. 2002;40(1):376-401.
48. Formaggia L, Vergara C. Prescription of general defective boundary conditions in fluid-dynamics. *Milan J Math*. 2012;80(2):333-350.
49. Karypis G, Kumar V. Multilevelk-way partitioning scheme for irregular graphs. *J Parallel Distrib Comput*. 1998;48(1):96-129.
50. Cai XC, Sarkis M. A restricted additive Schwarz preconditioner for general sparse linear systems. *SIAM J Sci Comput*. 1999;21(2):792-797.
51. Deparis S, Forti D, Quarteroni A. A rescaled localized radial basis function interpolation on non-Cartesian and nonconforming grids. *SIAM J Sci Comput*. 2014;36(6):A2745-A2762.

How to cite this article: Liu Y, Qi F, Cai X-C. An aneurysm-specific preconditioning technique for the acceleration of Newton-Krylov method with application in the simulation of blood flows. *Int J Numer Meth Biomed Engng*. 2023;e3771. doi:10.1002/cnm.3771